Check for updates

The difference of creep compliance for wood cell wall CML and secondary S_2 layer by nanoindentation

Dong Wang[1,2] · Lanying Lin[1] · Feng Fu[1]

Abstract Wood is generally considered a linear orthotropic viscoelastic. The creep of cell wall under long-term load is important for the deformation and destruction of wood. The aim of this study was to investigate the difference of creep compliance between compound middle lamella (CML) and secondary S_2 layers by nanoindentation creep testing. The results indicated that the creep compliance of cell wall under compression along grain increased with the maximum load and loading rate increasing. Furthermore, the creep compliances and creep compliance percentages of the CML layer were more than that of the secondary S_2 layer, and the viscoelastic behavior of the CML layer also was more sensitive to MC compared with the S_2 layer. Finally, the Burgers' model was appropriate for predicting the viscoelastic behavior of wood cell walls. The parameters of Burgers' model dropped markedly with increased MC. These parameters in the CML layer also were lower than those of S_2 layer. The differences of creep properties between the CML and S_2 layers can prove that the slippage failure of cell wall under compression along grain occurs in the S_2 layer.

Keywords Wood · Creep compliance · Compound middle lamella (CML) · Secondary S_2 layer

1 Introduction

Wood is extensively used in constructing structures and manufacturing products because it is environmentally friendly. However, it exhibits a so-called creep behavior under long-term loading due to its natural molecular structure and viscoelastic effect (Dinwoodie 1981; Salmén and Burgert 2009). The creep behavior of wood is the main factor that decreases the stiffness of wood construction under long-term loading and influences the quality of

Lanying Lin at: Xiangshan Road, Haidian District, Beijing, 100091, China

✉ L. Lin
  linly@caf.ac.cn

[1] Research Institute of Wood Industry, Chinese Academy of Forestry, Beijing, 100091, China

[2] Nanjing Forestry University of Materials and Science and Engineering, Nanjing, 210037, China

wood products. Many studies have also proven that the viscoelastic effect results in significant viscoelastic material failure, especially by the process of crack growth (Hoffmeyer and Davidson 1989; Dubois et al. 1998; Pitti et al. 2009).

Wood is a natural composite material with characteristic features at several hierarchical levels (Salmén and Burgert 2009). At the molecular level, wood mainly consists of cellulose, lignin, and hemicellulose. Elastic cellulose has almost no influence on the viscoelastic matrix (Toba et al. 2013), but hemicellulose and lignin show much more viscous behavior (Åkerholm and Salmén 2003; Schiffmann 2013; Borst et al. 2013). At the cellular level, the middle lamella (ML), as a bonded layer, connects two adjacent cell walls. The viscoelastic properties of different layers of wood cell walls are different due to the differences of their composite distributions and microfibril angles. Meng et al. (2015) reported the creep compliance of the S_2 layer of wood cell wall at different moisture contents (MCs). However, the viscoelastic properties of the ML or compound middle lamella (CML) layer were ignored. This work focuses on the differences of viscoelastic properties between S_2 and CML layers because it is important for the deformation and destruction of wood cell wall (Raghavan et al. 2012).

Moisture content (MC) is another important factor affecting wood viscoelasticity (Jin et al. 2016; Chassagne et al. 2005; Hering et al. 2012; Meng et al. 2015). The interaction between moisture changes and the mechanical behavior of wood remains a complicated issue, which greatly influences durability of wood and wood products. Wood chemical compositions and viscoelastic properties are important in explaining the reaction of this polymeric tissue to moisture changes and under a sustained load (Chassagne et al. 2005). A previous study suggested a linearly increasing viscoelastic compliance function with increasing MC (Hering et al. 2012).

The creep compliance $J(t)$, as a significant parameter for the evaluation of material viscoelastic behavior, is strictly defined as the change in strain as a function time under the instantaneous application of a constant stress, as stated in Eq. (1):

$$J(t) = \frac{\varepsilon(t)}{\sigma} \qquad (1)$$

This parameter mainly represents material deformation change under long-term loading and characterizes material time-dependent properties. For investigation of viscoelastic properties for material, a large number of macroscopic tests are available, which realize different types of loading: linear extension or compression, shear, and torsion (Ferry 1980). However, there are applications where these macroscopic tests cannot be applied in wood cell walls, where the material is too thin to use conventional tests, and in the field of micro-systems where additional lateral resolution is needed. For these applications, the nanoindentation technique gives access to small lateral and vertical dimensions by highly resolved measurements of load and displacement of a probe pressed into a surface. Nanoindentation has been widely applied to research on creep and stress relation tests of materials (Li and Bhushan 2002; Zhang et al. 2006) and also to study wood creep behavior (Zhang et al. 2012; Meng et al. 2015; Wang et al. 2016). The relative creep compliances with respect to time and stress were revealed only for the S_2 layer of the wood cell wall (Zhang et al. 2012). The creep compliance of the S_2 layer and its interrelation with chemical components was also investigated based on a nanoindentation creep test (Zhang et al. 2012; Wang et al. 2016).

In the current study, nanoindentation was applied to test creep compliance of the wood cell wall in order to analyze the viscoelasticity difference between CML and S_2 layers under different maximum loads, loading rates and MCs. The effects of composite distribution differences between CML and S_2 layers on cell wall viscoelasticity were investigated. The

Fig. 1 Nanoindentation load-displacement curves and indentation positions (Color figure online)
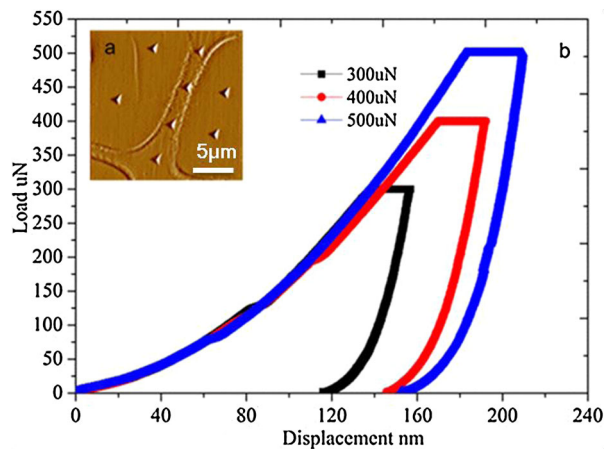
viscoelastic parameters of these two layers for different MCs also were calculated by the Burgers model.

2 Materials and methods

2.1 Materials

The wood material studied was taken at breast height from the mature green wood of a *Pinus massoniana* log (*Pinus massoniana Lamb.*, annual rings 75 ± 5, basic density was 0.51 ± 0.01 g/cm^3). The 45th growth ring of latewood was chosen to ensure accuracy of indentation position (Fig. 1a). Test specimens were conditioned to different MCs by placing them in sealed containers of saturated salt solutions. The nominal concentrations of the salt solutions used were 33% ($MgCl_2$), 76% ($NaCl$), and 93% (KNO_3). Absolutely dry wood was obtained above dry P_2O_5 in a vacuum desiccator. In most cases the specimens reached steady weights after 6 to 8 weeks of conditioning to reach the actual MCs (Absolutely dry, 5.9%, 13.4%, 19.6%).

2.2 Methods

2.2.1 Nanoindentation creep test

All experiments were conducted using a Hysitron TI 950 nanoindentation instrument. For the indentation a Berkovich diamond pyramid was used, with indentor tip radius of about 100 nm. In order to study the effect of maximum load and loading rate on creep compliance of wood cell wall, the MC of test specimens was absolutely dry. The creep compliance test was performed using the following maximum loads: 300 μN, 400 μN, and 500 μN; The standard holding time for these tests was 50 s; however, loading times or unloading times were varied at 5 s, 15 s, and 25 s, respectively. The indentation depths resulting from the above loading parameters took into consideration both surface roughness effect (indentation depth was more than 100 nm) and accuracy of CML layer indentation position (less than 300 nm, Fig. 1a). In order to study the effect of MC on creep compliance of wood cell wall, the parameters of nanoindentation creep testing as follows: maximum load was 400 μN,

holding time was 50 s, loading time and unloading time were 5 s. Inside the indentation chamber, the relative humidity to which samples needed to be subjected was maintained constantly and adjusted by using above-mentioned various saturated salt solutions and P_2O_5. All saturated salt solutions were maintained at a constant laboratory temperature of 25 ± 2 °C. Samples were stored in the indentation chamber and exposed to the environment 24 hours before the indentation test. At least 35 points in an S_2 or a CML layer of each sample were tested, and the creep compliance of S_2 or CML layer was obtained by averaging. The nanoindentation load-displacement curves and indentation positions are plotted in Fig. 1b.

2.2.2 Rheological models during nanoindentation

Wood is generally considered a linear orthotropic viscoelastic under some conditions (Schniewind and Barrett 1972). For the linear elastic properties, the relationship of stress-strain could be described by Hooke's law:

$$\sigma = E \cdot \varepsilon \tag{2}$$

Here E is the elastic modulus. On the other side, the viscous component is modeled as a dashpot, which is analogous to the energy dissipation. The stress and strain rate relationship can be expressed as follows:

$$\sigma = \eta \cdot \frac{d\varepsilon}{dt} \tag{3}$$

in which η is the viscosity of a material and $d\varepsilon/dt$ is the time derivative of the strain.

For a nanoindentation creep test, the stress is held constant, $\sigma = \sigma_0$, so the creep compliance $J(t)$ is defined by the following:

$$J(t) = \frac{\varepsilon(t)}{\sigma_0} \tag{4}$$

The load P, contact area A and indentation depth h are three important parameters in nanoindentation. The tip used in all experiments was a pyramidal indenter (Berkovich tip). Schiffmann (2006) has mentioned in his research that the representative stress is given by $\sigma = P/A$, and that the representative strain is defined by the following:

$$J(t) = \frac{A(t)}{2(1 - v^2)P_0 \tan \delta} \tag{5}$$

v is the Poisson ratio, and δ is the half opening angle of the indenter (71.15° in Berkovich). The load $P = P(0)$ was able to be obtained directly by the instrument. However, the contact area had to be calculated by the area function of the tip, which is described by a polynomial:

$$A = C_0 h_c^2 + C_1 h_c + C_2 h_c^{1/2} + C_3 h_c^{1/4} + C_4 h_c^{1/8} + C_5 h_c^{1/16} \tag{6}$$

Here C_i is the tip constant according to tip area function of standard quartz sample, as shown in Table 1 and h_c is the contact depth.

In the nanoindentation creep test, the holding load is constant and the contact area changes with time. Thus, h_c is given by

$$h_c(t) = h(t) - 0.75 \frac{P_0}{S_f} \tag{7}$$

Table 1 The tip constants according to tip area function of standard quartz sample

Tip constant	C_0	$C_1 \times 10^5$	$C_2 \times 10^7$	$C_3 \times 10^7$	$C_4 \times 10^8$	$C_5 \times 10^8$
Value	24.5000	−2.2592	2.4033	−2.9298	8.0796	−5.4589

Fig. 2 Schematic image of four-parameter Burgers' model
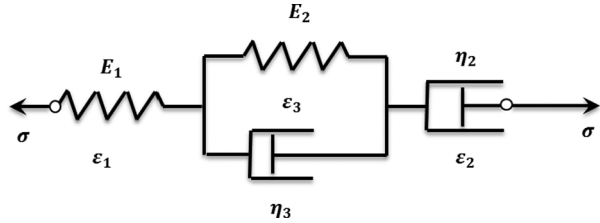
where $h(t)$ is the actual indentation depth during the holding period and S_f is the final stiffness calculated from the unloading segment.

2.2.3 Burgers' model

For the evaluation of different viscoelastic materials, Maxwell and Kelvin–Voigt models have been developed to predict the deformation of materials. In our analysis, both the Burgers model and generalized Maxwell model were applied to rationalize the experimental results and to investigate the wood cell wall. With reference to the Burgers model, a combination of Maxwell and a Kelvin element were taken into consideration with the schematic diagram shown in Fig. 2. The relationship between stress σ and deformation ε of such a material is given by Eqs. (8)–(10):

$$\sigma + p_1\dot{\sigma} + p_1\ddot{\sigma} = q_1\dot{\varepsilon} + q_2\ddot{\varepsilon} \tag{8}$$

where $\dot{\sigma}, \ddot{\sigma}, \dot{\varepsilon}, \ddot{\varepsilon}$ are defined as the first and second time derivatives of stress and deformation and can be expressed as

$$p_1 = \frac{\eta_2}{E_1} + \frac{\eta_2 + \eta_3}{E_3}; \qquad p_2 = \frac{\eta_2\eta_3}{E_1 E_3}; \qquad q_1 = \eta_2; \qquad q_2 = \frac{\eta_2\eta_3}{E_3} \tag{9}$$

where E_1, E_2 are the spring constants and η_2, η_3 are viscosities in Fig. 2.

In a creep experiment the stress $\sigma = $ const., so the first and second derivatives of stress are zero ($\dot{\sigma} = \ddot{\sigma} = 0$), and the differential Eq. (8) simplifies to

$$\sigma = q_1\dot{\varepsilon} + q_2\ddot{\varepsilon} \tag{10}$$

By applying this equation to Eq. (4), a solution can be written in the form of creep compliance:

$$J(t) = J_0 + J_1 \cdot t + J_2\big[1 - \exp(-t/\tau_0)\big] \tag{11}$$

where $J_0 = \frac{1}{K_1}$, $J_1 = \frac{1}{\eta_2}$, $J_2 = \frac{1}{K_2}$, $\tau_0 = \frac{\eta_3}{K_2}$, τ_0 is the retardation time, which describes the retarded elastic deformation of the Kelvin model in the Burgers model, and it is an important parameter that reflects the viscoelastic properties of a material.

2.2.4 Confocal Raman microscopy (CRM)

Raman spectra were acquired with a LabRam Xplora confocal Raman microscope (Horiba Jobin Yvon, Paris, France) equipped with a confocal microscope (BX51, Olympus, Japan) and motorized scan stage. To achieve high spatial resolution, an MPlan $100\times$ oil immersion microscope objective (numerical aperture (NA) = 1.4, Olympus) and a laser in the visible wavelength range ($\lambda = 532$ nm) were used. The linearly polarized laser light was focused with diffraction limited spot size of $0.61\lambda/NA$ onto samples and the Raman light was detected with an air cooled back-illuminated CCD behind the spectrograph. The laser power on the sample was ~ 8 mW. Chemical images were generated using a sum filter by integrating over defined wavenumber layers in the spectrum. The filter used to calculate the intensities within the chosen borders and the background was subtracted by taking the baseline from the first to the second border. The latewood cell wall layer was selected for Raman mapping at 0.4 µm step size with an integration time of 0.2 s. The chemical images enabled distinction between cell wall layers differing in cellulose and lignin with the color scale bar based on variation in Raman intensity. Average spectra from these layers of interest were extracted and baseline-corrected at 1800 cm^{-1} and 2200 cm^{-1} for detailed analysis. For sample preparation, cross sections of 10 µm thickness were cut from the samples using a rotary microtome (RM 2255, Leica, Germany). The cross sections were placed on glass slides and wetted with deuterium oxide. To avoid evaporation and drying out during measurements, the sections were covered with glass cover-slips (0.17 mm thickness) and sealed with nail polish.

2.2.5 Atomic force microscope-infrared spectroscopy analysis (AFM-IR)

AFM-IR is a hybrid technique that combines the spatial resolution of atomic force microscopy (AFM) with the chemical analysis capability of infrared (IR) spectroscopy. This technique can effectively distinguish different wall layers. A nanoIR2™-FS instrument (Anasys Instruments Corp., USA) was used to collect the spatially resolved IR spectra. The horizontal resolution was 10 nm, and a line-scanning model was selected. The flat silicon substrate with the sample was mounted on the sample stage of the AFM-IR instrument. Using an incident light micrograph as a guide, locations of the cell wall S_2 and CML layers could be examined. The AFM-IR spectra were collected from 1000 to 1800 cm^{-1}. AFM-IR spectra were collected at secondary S_2 and CML layers. The spectra were baseline-corrected at 1800 cm^{-1}. Each spectrum of an S_2 or a CML layer was calculated from averages of 15 spectra of the same layer. Cross sections of 300 nm thickness were cut from the samples using a rotary microtome (RM 2255, Leica, Germany) and diamond knife. The slice was transferred onto a flat calcium fluoride (CaF) window with dimensions of 5 mm $\times$ 5 mm.

3 Results and discussion

3.1 The differences of wood chemical composites distribution between CML and S_2 layers

The Raman spectrogram shows cellulose and lignin distribution regularities within wall layers (Fig. 3). The characteristic band of lignin consists of the aromatic skeletal vibrations close to 1600 cm^{-1} (Agarwal 2019). The highest level of lignin concentration occurred in the CML layer and the lowest level was found in the S_2 layers from the peak intensity at
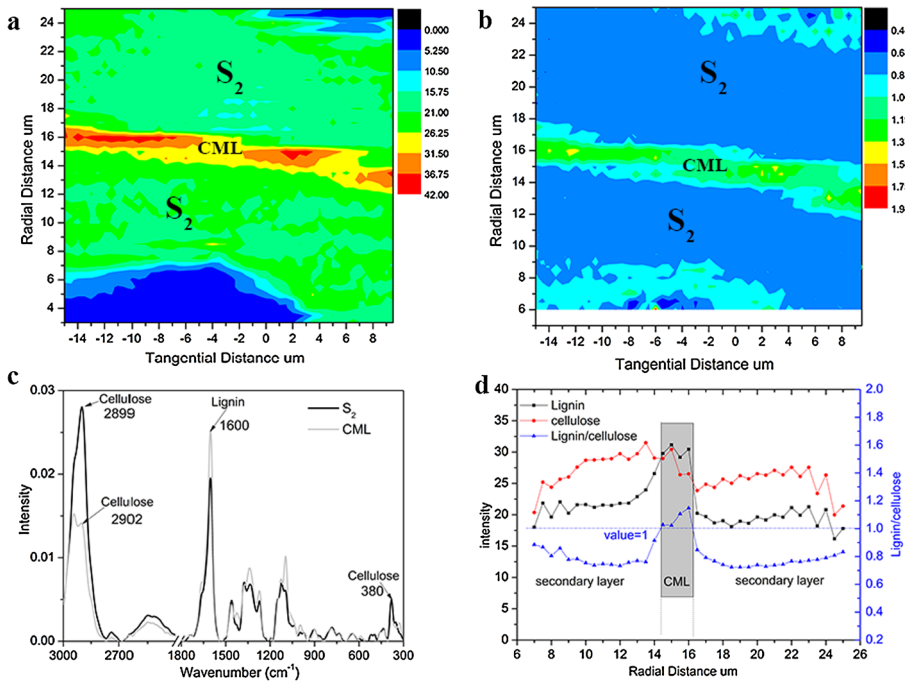
Fig. 3 CRM spectra (**a**) lignin distribution (I_{1600}); (**b**) lignin/cellulose distribution (I_{1600}/I_{2899}); (**c**) CRM spectra between S_2 and CML layers; (**d**) the distributions of lignin, cellulose and lignin/cellulose in the direction of wall thickness (Color figure online)

1600 cm^{-1} (Fig. 3a and Fig. 3c). Similar findings were reported by previous studies (Ji et al. 2014; Wang et al. 2014). The vibration bands of cellulose, specifically glucoside bond at 380 cm^{-1}, the C–H and C–H$_2$ stretchings at 2895–2902 cm^{-1}, were monitored (Agarwal 2019). The highest concentration of cellulose was observed in the S_2 layer (Fig. 3c and Fig. 3d). This is consistent with the wood cell wall structure that had been previously reported (Schmidt et al. 2009; Wang et al. 2014). Amorphous matrix relative proportion (lignin/cellulose) changes within wall layers were consistent with lignin distribution (Fig. 3b). Figure 4 illustrates a series of AFM-IR spectra (Fig. 4d) for secondary S_2 and CML layer. The black IR spectra are recorded in the CML layer and the gray spectra in the secondary S_2 layers (Fig. 4). The band at 1732 cm^{-1} was indicative of the C=O stretching vibration in the acetyl group of hemicellulose (Marcott et al. 2014). The highest concentration of xylan was observed in the CML layer (Fig. 4). The spatial distribution of lignin was visualized based on the peak at 1596 cm^{-1} and 1509 cm^{-1} ascribed to the symmetric stretching of the C=C bonds in the aromatic ring. The result indicated that the highest concentration of lignin also was observed in the CML layer (Fig. 4).

3.2 The effect of maximum load and loading rate on creep compliance

Creep experiments conducted with a pyramid tip induced a load-dependent response but also a loading-rate-dependent response. The creep compliance was calculated by Eqs. (5)–(7). This point in illustrated in Fig. 5 where $J(t)$ is shown for different maximum loads (Fig. 5a) and loading rates (Fig. 5b). Increase of holding time induced an increase in $J(t)$,

**Fig. 4** AFM-IR spectra of S_2 and CML layers
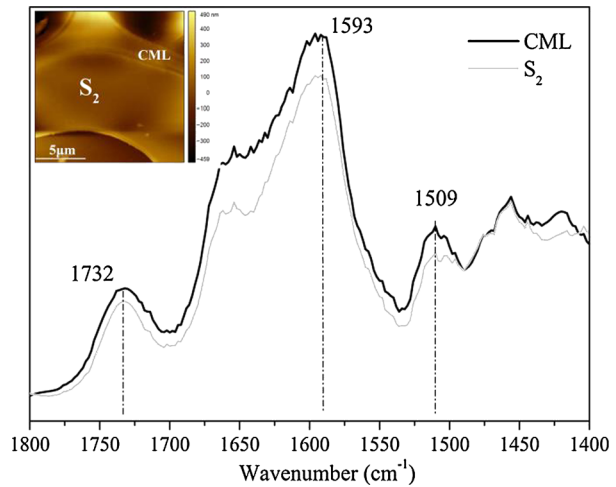
but this trend became slow with holding time increase because the material became stronger with compression strain increase. As the maximum loads increase from 300 μN to 500 μN, the creep compliances at the beginning of the holding period increased from 0.35 GPa^{-1} to 0.42 GPa^{-1} for the S_2 layer, and from 0.48 GPa^{-1} to 0.56 GPa^{-1} for CML layer (Fig. 5a). This result indicated that load was the main cause of deformation. The creep compliance percentage is defined as the compliance difference between the beginning and ending of the holding period divided by the creep compliance at the beginning of holding (Meng et al. 2015). As the maximum loads increase from 300 μN to 500 μN, the creep compliance percentages of the S_2 layer were 25.71%, 28.21% and 23.81%; and for the CML layer the percentages were 31.25%, 32.69%, and 22.22% (Fig. 5a). When the maximum load was 400 μN, the creep compliance percentage was the largest. The most likely reason for this is that the 300 μN load produces smaller strain at the beginning of the holding period, but the 500 μN load produces hardening deformation.

The increase in loading rates from 12 μN/s to 60 μN/s, namely the decrease in loading times from 25 s to 5 s, induced an increase in $J(t)$ (Fig. 5b). For different loading ratios, the creep compliances at the beginning of the holding period had no significant differences. However, as loading ratios increase from 12 μN/s to 60 μN/s, the creep compliance percentages of the S_2 were 20.61%, 22.66% and 24.35%, respectively, and for the CML layer were 16.07%, 21.14%, and 35.96% (Fig. 5b). This result indicated that the creep compliance percentage increased with loading rates increase. Rapid loading to P_0 minimizes energy dissipation through viscous mechanisms, while slow loading to P_0 enables concurrent elastic and viscous responses prior to creep (Zhang et al. 2012).

### 3.3 The effect of MC on creep compliance

The experimental creep compliance of wood cell walls with different MCs is shown in Fig. 6. The creep compliances of cell walls were increased with MCs ranging from absolutely dry to 19.6%. The creep compliance of the S_2 layer at the onset of unloading increased from 0.38 GPa^{-1} in the oven-dried condition to 0.52 GPa^{-1} under 19.6% MC, and the creep compliance of the CML layer increased from 0.54 GPa^{-1} to 0.74 GPa^{-1}. The creep compliance percentages of the S_2 layer were 23.33%, 32.26%, 36.36% and 36.84% for different
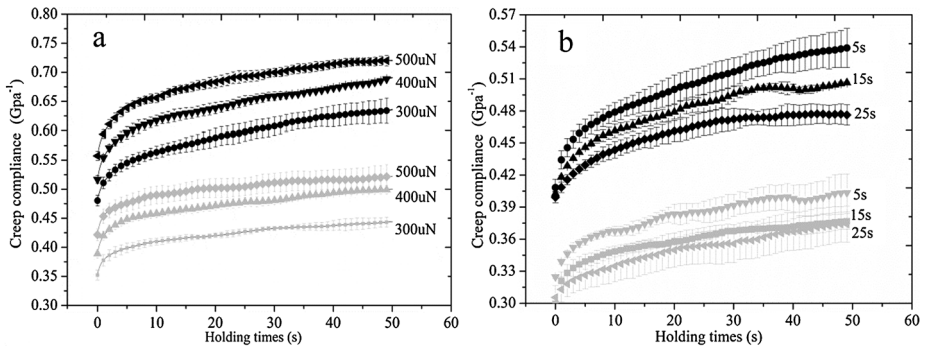
Fig. 5 Creep compliance with respect to maximum load and loading rate (black: CML layer, gray: S$_2$ layer; **a**: loading time 5 s, **b**: maximum load 300 μN)

Fig. 6 The creep compliance of cell walls with different moisture contents (black: CML, gray: cell wall S$_2$ layer)
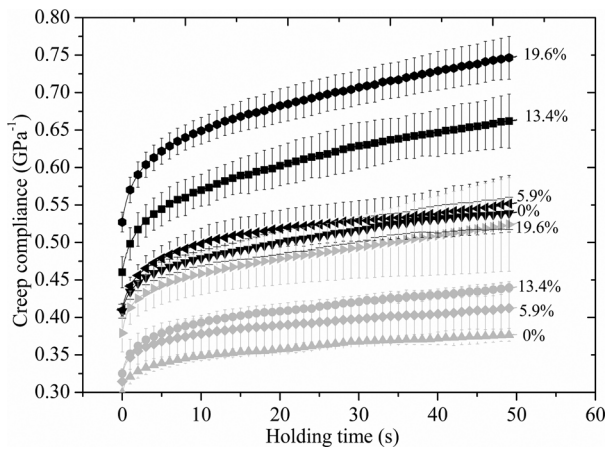
MCs samples, and the creep compliance percentage increased with MC increasing. Furthermore, the creep compliance percentages of the CML layer were 28.57%, 34.15%, 43.48% and 42.31% for different MCs samples. In other words, the samples with higher MC deformed more when subjected to the constant load. In a wood polymer chain, the induction of MC tends to increase the number of water molecules at the interface between amorphous hemicellulose and crystal cellulose and to enlarge the inter-chain distance, which weakens the structural continuity and reduces the resistance of the wood cell wall to creep (Meng et al. 2015). The creep compliances and creep compliance percentages of the CML layer under different MCs were more than that of the S$_2$ layer. This result indicated that the creep behavior of the CML layer is more sensitive to MC than the S$_2$ layer.

The viscoelastic behavior of wood cell wall in terms of stress and strain can be described by the four parameters Burgers model by means of the observed $J(t)$, which were obtained by fitting the creep compliance curve to Eq. (10). The experimental creep compliance data for the CML and S$_2$ layers, together with Burgers' model, predicted creep compliance, as shown in Fig. 7 (red dot dash line). The R^2 correlation coefficient was over 0.99 for all samples, indicating that Burgers' model was appropriate for predicting wood cell wall viscoelastic behavior. The four-parameter Burgers' model is that the fitting parameters could be interpreted physically as an instantaneous elastic deformation, followed by a viscoelastic

Table 2 Elastic and viscosity coefficients from Burgers' fit curves: spring constant, viscosity, and viscoelasticity (maximum load: 400 μN; loading time: 5 s)

| MC	Absolutely dry		5.9%		14.3%		19.6%	
	CML	S_2	CML	S_2	CML	S_2	CML	S_2
K_1 (GPa)	2.31	3.22	2.36	3.00	2.08	2.96	1.83	2.54
K_2 (GPa)	15.18	29.45	13.88	25.06	12.08	20.30	11.04	19.24
η_2 (GPa)	1250.00	1473.12	917.43	1251.58	480.77	917.43	436.68	617.28
η_3 (GPa)	196.40	113.90	59.98	83.35	59.83	76.76	44.86	54.65

deformation and viscous deformation. The parameters in Burgers' model include the modulus of elasticity (E_1), modulus of viscoelasticity (E_2), and coefficient of viscosity (η_2 and η_3), as listed in Table 2. Apparently, the viscoelastic behavior of the CML layer is sensitive to the MC compared with the S_2 layer. It was observed that in the moisture range of the current study, elasticity, viscoelasticity, and viscosity parameters of wood cell wall were decreased with MC increasing. When water entered into matrix and cellulose amorphous layers, the distance between macromolecular chains increased, indicating that slippage between macromolecules increased under load. Thus, the ratio of wood viscosity to rheology deformation ($d\varepsilon/dt$) was larger, and viscosity coefficient (η_2) was decreased (Meng et al. 2015; Cousins 1976, 1978). Furthermore, the absorption of matrix led to its size change and to cellulose lateral elongation that increased axial strain (Pitti et al. 2009). Finally, water easily enters cellulose amorphous layers and surfaces, leading to the decrease in cellulose stiffness.

3.4 Creep compliance differences between the CML and S_2 layers

The creep compliances and creep compliance percentages of the CML layer were higher than that of the S_2 layer in different maximum loads, loading rates and MCs (Fig. 5, Fig. 6). The E_1, E_2, η_1, and η_2 of the CML layer also were lower than that of the S_2 layer (Table 2). The main reasons for this were that the highest level of lignin and hemicellulose concentration occurred in the CML layer; the highest level of cellulose was found in the S_2 layer and microfibrils arrangement were parallel to the cell axis (Fig. 3, Fig. 4d). The measurements indicated that lignin and hemicellulose showed much more viscosity behavior than did cellulose (Åkerholm and Salmén 2003). Brémaud et al. (2013) also found that an increased lignin/cellulose ratio should result in an increased viscosity. Furthermore, the main ingredient of the primary wall is pectin, which has strong hydrophilicity and plasticity, and could lead to much more viscosity. Additionally, the angle of the cellulose microfibrils to the longitudinal direction within the S_2 layer ranged from 10° to 30°, the stiffness of cellulose in the longitudinal direction was greater. The increasing trend of the creep compliance percentages of CML layer as MC increase was more than that of the S_2 layer. The viscoelastic behavior of the CML layer is more sensitive to the MC compared with the S_2 layer, mainly because of higher concentrations of hemicellulose in the CML layer. As a stress transmitter and weak interface, it allows the adjacent secondary wall to incur a greater shear slip. When wood was subjected to long-term compression stress parallel to grain, the creep deformation occurred and led to the formation of slip planes in the cell wall S_2 layer (Hoffmeyer and Davidson 1989; Gong and Smith 2004).

Fig. 7 Representative fit curve of Burgers' model to the holding portion of an indentation curve (Color figure online)

J(t)=0.08275×(1 - exp(-0.20198×t))+0.00208×t+0.48034

J(t)=0.04926×(1 - exp(-0.26448×t))+0.00109×t+0.33762
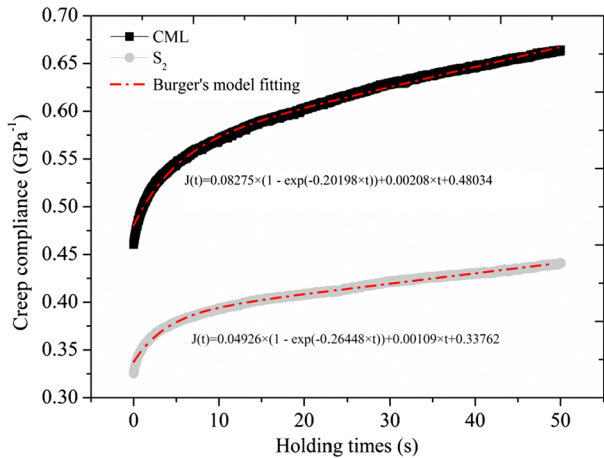
4 Conclusion

The creep compliance of cell wall under compression along grain increased with the maximum load and loading rate increasing. Furthermore, the creep compliances and creep compliance percentages of the CML layer were more than that of the secondary S_2 layer layers under all test conditions and MCs. Furthermore, Burgers' model was appropriate for predicting the viscoelastic behavior of cell walls. The parameters of Burgers' model dropped markedly with increased MC. These parameters in the CML layer also were lower than those of S_2 layer. When wood subjected to compression stress parallel to grain, the differences of creep compliance between the CML and S_2 layers lead to stress concentration and slippage failure of cell wall occurring in the S_2 layer.

Publisher's Note   Springer Nature remains neutral with regard to jurisdictional claims in published maps and institutional affiliations.

References

Agarwal, U.P.: Analysis of cellulose and lignocellulose materials by Raman spectroscopy: a review of the current status. Molecules **24**(9), 1659 (2019)

Åkerholm, M., Salmén, L.: The oriented structure of lignin and its viscoelastic properties studied by static and dynamic FT-IR spectroscopy. Holzforschung **57**(5), 459–465 (2003)

Borst, K.D., Jenkel, C., Montero, C., Colmars, J., Gril, J., Kaliske, M., Eberhardsteiner, J.: Mechanical characterization of wood: an integrative approach ranging from nanoscale to structure. Comput. Struct. **127**(127), 53–67 (2013)

Brémaud, I., Ruelle, J., Thibaut, A., Thibaut, B.: Changes in viscoelastic vibrational properties between compression and normal wood: roles of microfibril angle and of lignin. Holzforschung **67**(1), 75–85 (2013)

Chassagne, P., Saïd, E.B., Jullien, J.F., Galimard, P.: Three dimensional creep model for wood under variable humidity-numerical analyses at different material scales. Mech. Time-Depend. Mater. **9**(4), 1–21 (2005)

Cousins, W.J.: Elastic modulus of lignin as related to moisture content. Wood Sci. Technol. **10**(1), 9–17 (1976)

Cousins, W.J.: Young's modulus of hemicellulose as related to moisture content. Wood Sci. Technol. **12**(3), 161–167 (1978)

Dinwoodie, J.M.: Timber, Its Nature and Behavior. Spon Press, New York (1981)

Dubois, F., Chazal, C., Petit, C.: A finite element analysis of creep-crack growth in viscoelastic media. Mech. Time-Depend. Mater. **2**(3), 269–286 (1998)

Ferry, J.D.: Viscoelastic Properties of Polymers. John Wiley & Sons, New York (1980)

Gong, M., Smith, I.: Effect of load type on failure mechanisms of spruce in compression parallel to grain. Wood Sci. Technol. **37**(5), 435–445 (2004)

Hering, S., Keunecke, D., Niemz, P.: Moisture-dependent orthotropic elasticity of beech wood. Wood Sci. Technol. **46**(5), 927–938 (2012)

Hoffmeyer, P., Davidson, R.W.: Mechano-sorptive creep mechanism of wood in compression and bending. Wood Sci. Technol. **23**(3), 215–227 (1989)

Ji, Z., Ma, J., Xu, F.: Multi-scale visualization of dynamic changes in poplar cell walls during alkali pretreatment. Microsc. Microanal. **20**(2), 566–576 (2014)

Jin, F., Jiang, Z., Wu, Q.: Creep behavior of wood plasticized by moisture and temperature. BioResources **11**(1), 827–838 (2016)

Li, X., Bhushan, B.: A review of nanoindentation continuous stiffness measurement technique and its applications. Mater. Charact. **48**(1), 11–36 (2002)

Marcott, C., Lo, M., Hu, Q., Dillon, E., Kjoller, K., Prater, C.B.: Nanoscale infrared spectroscopy of polymer composites. Am. Lab. **46**(3), 23–25 (2014)

Meng, Y., Xia, Y., Young, T.M., Cai, Z., Wang, S.: Viscoelasticity of wood cell walls with different moisture content as measured by nanoindentation. RSC Adv. **5**(59), 47538–47547 (2015)

Pitti, R.M., Dubois, F., Pop, O., Absi, J.: A finite element analysis for the mixed mode crack growth in a viscoelastic and orthotropic medium. Int. J. Solids Struct. **46**(20), 3548–3555 (2009)

Raghavan, R., Adusumalli, R.B., Buerki, G., Hansen, S., Zimmermann, T., Michler, J.: Deformation of the compound middle lamella in spruce latewood by micro-pillar compression of double cell walls. J. Mater. Sci. **47**(16), 6125–6130 (2012)

Salmén, L., Burgert, I.: Cell wall features with regard to mechanical performance. A review COST Action E35 2004–2008: wood machining–micromechanics and fracture. Holzforschung **63**(2), 121–129 (2009)

Schiffmann, K.I.: Nanoindentation creep and stress relaxation tests of polycarbonate: analysis of viscoelastic properties by different rheological models. Z. Met.kd. **97**(9), 1199–1211 (2006)

Schiffmann, K.I.: Nanoindentation creep and stress relaxation tests of polycarbonate: analysis of viscoelastic properties by different rheological models. Z. Met.kd. **97**(9), 1199–1211 (2013)

Schmidt, M., Schwartzberg, A.M., Perera, P.N.: Label-free in situ imaging of lignification in the cell wall of low lignin transgenic Populus trichocarpa. Planta **230**(3), 589–597 (2009)

Schniewind, A.P., Barrett, J.D.: Wood as a linear orthotropic viscoelastic material. Wood Sci. Technol. **6**(1), 43–57 (1972)

Toba, K., Yamamoto, H., Yoshida, M.: Crystallization of cellulose microfibrils in wood cell wall by repeated dry-and-wet treatment, using X-ray diffraction technique. Cellulose **20**(2), 633–643 (2013)

Wang, X., Keplinger, T., Gierlinger, N., Burgert, I.: Plant material features responsible for bamboo's excellent mechanical performance: a comparison of tensile properties of bamboo and spruce at the tissue, fibre and cell wall levels. Ann. Bot. Lond. **114**(8), 1627–1635 (2014)

Wang, X.Z., Li, Y.J., Deng, Y.H., Yu, W.W., Xie, X.Q., Wang, S.Q.: Contributions of basic chemical components to the mechanical behavior of wood fiber cell walls as evaluated by nanoindentation. BioResources **11**(3), 6026–6039 (2016)

Zhang, C.Y., Zhang, Y.W., Zeng, K.Y., Shen, L.: Characterization of mechanical properties of polymers by nanoindentation tests. Philos. Mag. **86**(28), 4487–4506 (2006)

Zhang, T., Bai, S.L., Zhang, Y.F., Thibaut, B.: Viscoelastic properties of wood materials characterized by nanoindentation experiments. Wood Sci. Technol. **46**(5), 1003–1016 (2012)